Effect of Agitation on the Fluidization Behavior of a Gas–Solid Fluidized Bed with a Frame Impeller

Jia-Jun Wang, Ying Han, Xue-Ping Gu, and Lian-Fang Feng
State Key Laboratory of Chemical Engineering, Dept. of Chemical and Biological Engineering, Zhejiang University, Hangzhou 310027, P.R. China

Guo-Hua Hu
CNRS-Université de Lorraine, Laboratory of Reactions and Process Engineering, UPR 3349, ENSIC, 1 Rue Grandville, BP 20451, Nancy, F-54000, France

DOI 10.1002/aic.13893
Published online August 17, 2012 in Wiley Online Library (wileyonlinelibrary.com).

The effect of agitation on the fluidization performance of a gas–solid fluidized bed with a frame impeller is experimentally and numerically investigated. A 3-D unsteady computational fluid dynamics method is used, combining a two-fluid model and the kinetic theory of granular flow. The rotation of the impeller is implemented with a multiple reference frame method. The numerical model is validated using experimental data of the bed pressure drop and pressure fluctuation. Although the minimum fluidizing velocity and bed pressure drop are independent of the impeller agitation, a sufficiently high agitation speed yields higher fluidization performance with reduced bubble diameters and internal circulations of particles. The fluidized bed can be divided into three zones: inlet zone where the gas distribution plays a major role, agitated fluidization zone where the impeller agitation has a positive effect on fluidization, and free fluidization zone where the impeller agitation has no effect on fluidization. © 2012 American Institute of Chemical Engineers *AIChE J,* 59: 1066–1074, 2013
Keywords: computational fluid dynamics, fluidized bed, solid volume fraction, multiphase flow, agitation

Introduction

A large number of industrial processes are conducted in fluidized beds due to their simple structures and excellent mass and heat-transfer characteristics. Fluidized beds are the cores of various commercial olefin polymerization processes such as Hypol, Innovene, and Unipol. For gas-phase polymerization processes, monomer(s) in the gas phase must diffuse through the boundary layers around catalyst particles as well as their pores to reach active sites where the polymerization takes place. Therefore, good fluidization quality is necessary for ensuring gas–solid contact and mass transfer. However, it is difficult to maintain smooth fluidization due to the agglomeration of polymer particles, especially for high-impact polypropylene ones whose surfaces may be sticky.

Mechanical agitation has been used to prevent particles from agglomeration in a fluidized bed and improve fluidization quality. It is useful for many fluidizing processes using particles with large cohesive force,[1–3] such as granulation,[4,5] drying,[6] and crystallization.[7] Various types of agitators have been used in gas–solid processes. The combination of rods and curved blades is suitable for particle segregation,[8] whereas circular plate blades are often used for granulation.[4,5] Fluidization of Geldart C particles may exhibit an unstable hydrodynamic behavior and could be improved by a semi-inverted-anchor type of agitator.[2] Our previous experimental works studied the effects of the agitation speed and agitator type on the fluidization quality in polymerization reactors.[9–12]

As the first study on a fluidized bed with an oscillating stirrer[13] in 1950s, the majority of experimental investigations have been focused on the effect of the installation manner and rotating direction of blades on the pressure drop.[2,8,14–16] Power requirements for agitating solid beds have also attracted much attention and correlations have been proposed.[17–19]

It is often difficult to acquire detailed information on fluidization due to the limitations of measurement techniques. As such, computational fluid dynamics (CFD) has been becoming a potential tool to predict complicated flows in gas–solid fluidized beds, providing local and instantaneous information. Most early CFD studies were focused on model improvement[20–22], hydrodynamics and the effects of operating parameters on the fluidization performance in traditional fluidized beds.[23,24]

CFD simulations of gas–solid fluidized beds with agitators are rare due to the complexities of the reactor structure and the difficulties of convergence of the computation. Kim and Han[25] implemented a simplified CFD computation to simulate the velocity field using a fan model.[26] A pitched-blade turbine agitator was installed to prevent agglomeration and enhance fluidization. Shi et al.[27] described the gas–solid flow in a fluidized bed with an agitator using a two-fluid model

Correspondence concerning this article should be addressed to L.-F. Feng at fenglf@zju.edu.cn.

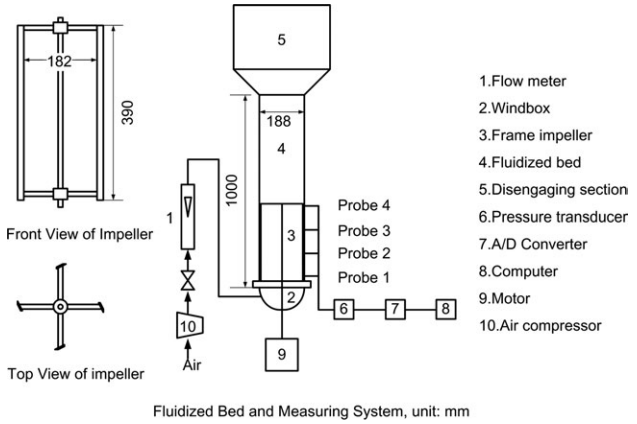

Figure 1. Schematic diagram of the experimental set up for the fluidized bed with a frame impeller.

and a multiple reference frame (MRF) method. They found that compared with a traditional fluidized bed, agitation improved the fluidization efficiency, but decreased the overall fluidization quality. However, only one set of operating conditions with an agitation speed of 1.05 rad/s was considered and the model was not validated experimentally. Therefore, the influence of the agitation speed on the fluidization performance was unclear.

Most of the agitators mentioned above were small in diameter and short in height.[1,3,14,25] They were applicable for drying, granulation, and crystallization processes. For polymerization processes, agitators capable of covering the whole reactor volume are preferred to scrape adhesive polymer particles from the reactor wall and improve fluidization quality. Therefore, a question rises of how to design, optimize and scale up a fluidized bed with a large diameter impeller for olefin polymerization.

In this work, the influence of agitation of a large diameter frame impeller on the fluidization behavior is investigated experimentally and numerically. A three-dimensional (3-D) time-dependent CFD model is presented based on the Eulerian-Eulerian two-fluid model coupled with the kinetic theory of granular flow (KTGF). A MRF approach is incorporated in the numerical model to deal with the rotating region. The bed pressure drop, minimum fluidizing velocity, pressure fluctuation, distributions of the particle velocity and solid volume fraction for different agitation speeds are investigated in this article.

Experimental

Figure 1 shows the fluidized bed with a frame impeller used in this study. The fluidized bed column was 188 mm in diameter and 1000 mm in height. Four pressure transducers (KYBD14, Advantech, China) were installed along the column at the reactor elevation of 35, 150, 265, and 380 mm, corresponding to probes 1–4, respectively. The voltage signals from the pressure transducers were transmitted to a personal computer with a data sampling rate of 200 Hz. The four-blade frame impeller with a diameter of 182 mm and a height of 390 mm was mounted at the bottom of the bed with a clearance of 10 mm. In the case of industrial applications, four 45° pitched blades were used to scrape sticky particles from the wall. Therefore, the agitation speed did not have to be high and was limited to 6.28 rad/s.

Polypropylene particles (Sinopec, China) with an average diameter of 1.130 mm and a density of 997.9 kg/m^3 were used as the bed materials. They could be classified as Geldart D particles. The initial bed height was 400 mm. Experiments were conducted at room temperature and atmospheric pressure. Compressed air from two compressors was used as the fluidizing gas. Its flow rate was measured by a standard orifice flow meter and the signals were delivered to the computer in the form of voltage. Table 1 shows the operating conditions.

Numerical Models

Eulerian–Eulerian two-fluid model

The simulation work was carried out in an Eulerian–Eulerian frame using the two-fluid model. The fluidizing gas was treated as an ideal one. The gas and solid phases are regarded as interpenetrating continua, both with their own volumes, velocities, and pressures. A set of continuity and momentum equations for both phases constitute the governing equations for the gas–solid system. The continuity equation for phase i (i = g for the gas phase and i = s for the solid one) is given by

$$\frac{\partial}{\partial t}(\rho_i \varepsilon_i) + \nabla \cdot (\rho_i \varepsilon_i \overline{v}_i) = 0 \tag{1}$$

When the mass transfer between phases, the external body force, the lift force and the virtual mass force are neglected, the conservations of momentum for the two phases have similar forms, given by

$$\frac{\partial}{\partial t}(\rho_g \varepsilon_g \vec{v}_g) + \nabla \cdot (\rho_g \varepsilon_g \vec{v}_g \vec{v}_g) = -\varepsilon_g \nabla P + \nabla \cdot \bar{\bar{\tau}}_g - K_{gs}(\vec{v}_g - \vec{v}_s) + \rho_g \varepsilon_g g \tag{2}$$

$$\frac{\partial}{\partial t}(\rho_s \varepsilon_s \vec{v}_s) + \nabla \cdot (\rho_s \varepsilon_s \vec{v}_s \vec{v}_s) = -\varepsilon_s \nabla P - \nabla P_s + \nabla \cdot \bar{\bar{\tau}}_s + K_{gs}(\vec{v}_g - \vec{v}_s) + \rho_s \varepsilon_s g \tag{3}$$

where $\bar{\bar{\tau}}_i$ is the stress–strain tensor for phase i, written as

$$\bar{\bar{\tau}}_g = \varepsilon_g \mu_g (\nabla \vec{v}_g + \nabla \vec{v}_g^T) \tag{4}$$

$$\bar{\bar{\tau}}_s = \varepsilon_s \mu_s (\nabla \vec{v}_s + \nabla \vec{v}_s^T) + \varepsilon_s (\lambda_s - \frac{2}{3}\mu_s) \nabla \cdot \vec{v}_s \bar{\bar{I}} \tag{5}$$

where $\bar{\bar{I}}$ is the identity matrix; μ_i and λ_i are shear viscosity and bulk viscosity of phase i, respectively, and their detailed forms will be given later.

KTGF

The constitutive equations derived from the kinetic theory are introduced to close the momentum equation for the solid phase. The KTGF describes the effective solid phase stress and pressure. In addition, the conservation of the kinetic

Table 1. Operating Conditions

Parameter	Unit	Value
Particle diameter	mm	1.13
Particle density	kg/m^3	997.9
Particle packing density	kg/m^3	624.6
Gas velocity	m/s	0.85
Agitation speed	rad/s	0, 1.05, 2.09, 3.14, 4.17, 6.28
Initial bed height	mm	400

energy of moving particles is given based on the granular temperature, Θ_s, as[28]

$$\frac{3}{2}\left[\frac{\partial}{\partial t}(\varepsilon_s\rho_s\Theta_s)+\nabla\cdot(\varepsilon_s\rho_s \text{ vs }\Theta_s)\right]=(-P_s\bar{\bar{I}}+\bar{\bar{\tau}}_s):\nabla\vec{v}_s+\nabla\cdot(k_{\Theta_s}\nabla\Theta_s)-\gamma\Theta_s+\phi_{gs} \quad (6)$$

where the term $k_{\Theta_s}\nabla\Theta_s$ stands for the diffusive flux of granular energy, and $k_{\Theta s}$ is described by Gidaspow et al.[29]

$$k_{\Theta_s}=\frac{150d_s\rho_s\sqrt{\Theta_s\pi}}{384(1+e_{ss})g_{0,ss}}\left[1+\frac{6}{5}\varepsilon_s g_{0,ss}(1+e_{ss})\right]^2+2\rho_s\varepsilon_s^2 d_s(1+e_{ss})g_{0,ss}\sqrt{\frac{\Theta_s}{\pi}} \quad (7)$$

The collisional dissipation of energy, $\gamma\Theta_s$, in Eq. 6 is the dissipation rate of the solid phase caused by particle–particle collisions. The correlation is developed by Lun et al.,[30] written as

$$\gamma\Theta_s=\frac{12(1-e_{ss}^2)g_{0,ss}}{d_s\sqrt{\pi}}\rho_s\varepsilon_s^2\Theta_s^{3}/2 \quad (8)$$

The transfer of the kinetic energy of random fluctuations in particle velocity from the solid phase to the gas one is denoted as ϕ_{gs}[29]

$$\phi_{gs}=-3K_{gs}\Theta_s \quad (9)$$

In Eq. 3, the solids pressure, P_s, is derived from Lun et al.[30]

$$P_s=\varepsilon_s\rho_s\Theta_s+2\varepsilon_s^2\rho_s(1+e_{ss})g_{0,ss}\Theta_s \quad (10)$$

where $g_{0,ss}$ and e_{ss} denote the radial distribution function and the coefficient of restitution for particle collisions, respectively. In this work, values ranging from 0.8 to 0.95 for the restitution coefficient were tested, but no significant differences on fluidization were found. $g_{0,ss}$ describes the probability of particle collisions and is expressed as[31]

$$g_{0,ss}=\left[1-\left(\frac{\varepsilon_s}{\varepsilon_{s,max}}\right)^{\frac{1}{3}}\right]^{-1} \quad (11)$$

The solids bulk viscosity, λ_s, in Eq. 5, quantifies the resistance of the granular particles to compression and expansion and is expressed as[30]

$$\lambda_s=\frac{4}{3}\varepsilon_s\rho_s d_s(1+e_{ss})g_{0,ss}\sqrt{\frac{\Theta_s}{\pi}} \quad (12)$$

The solids shear viscosity, μ_s, in Eq. 5 is given as

$$\mu_s=\frac{10\rho_s d_s\sqrt{\Theta_s\pi}}{96\varepsilon_s(1+e_{ss})g_{0,ss}}\left[1+\frac{4}{5}\left(1+e_{ss}\right)g_{0,ss}\varepsilon_s\right]^2+\frac{4}{5}\varepsilon_s\rho_s d_s(1+e_{ss})g_{0,ss}\left(\frac{\Theta_s}{\pi}\right)^{1/2}+\frac{P_s\sin\varphi}{2\sqrt{I_{2D}}} \quad (13)$$

where the first term on the right hand is the kinetic part of shear viscosity derived from Gidaspow et al.,[29] the second one refers to the collisional part,[26,29] and the third one the stress due to friction between particles.[32]

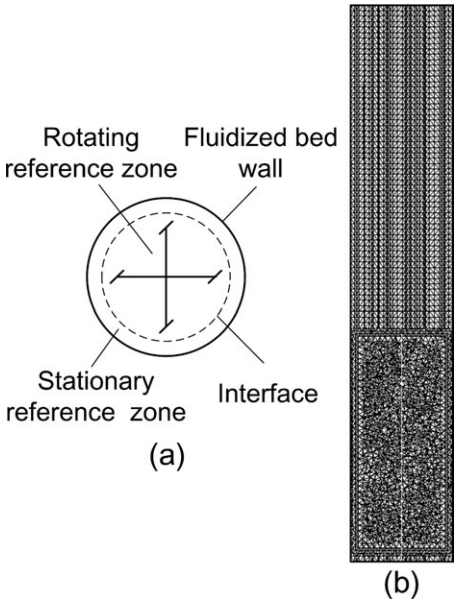

Figure 2. Two reference zones of MRF for the fluidized bed with a frame impeller (a) and grid distribution (b).

Drag force model

The momentum exchange between phases, K_{gs} in Eqs. 2 and 3, can be estimated by an empirical drag law, which is very important for predicting the fluidization behavior. The commonly used drag laws include Wen and Yu model,[33] Gidaspow model,[34] and Syamlal and O'Brien model.[35] In this work, preliminary simulations were conducted using these three drag models and no significant differences were found in terms of bubble properties. This is in agreement with the conclusion of Asegehegn et al.[36] Therefore, our work used the Gidaspow drag model as it was preferred for densely packed fluidized beds[37]

$$\text{At } \varepsilon_g\geq 0.8, K_{gs}=\frac{3}{4}C_D\frac{\varepsilon_s\varepsilon_g\rho_g\left|\vec{v}_g-\vec{v}_s\right|}{d_s}\varepsilon_g^{-2.65} \quad (14)$$

$$\begin{aligned} C_D&=\tfrac{24}{\varepsilon_g Re_s}(1+0.15(\varepsilon_g \text{Re}_s)^{0.687}); && \text{Re}_s<1000\\ C_D&=0.44; && \text{Re}_s\geq 1000 \end{aligned} \quad (15)$$

$$\text{where Re}_s=\frac{\rho_g d_s\left|\vec{v}_g-\vec{v}_s\right|}{\mu_g} \quad (16)$$

$$\text{At } \varepsilon_g<0.8,\ K_{gs}=150\frac{\varepsilon_s(1-\varepsilon_g)\mu_g}{\varepsilon_g d_s^2}+1.75\frac{\rho_g\varepsilon_s\left|\vec{v}_g-\vec{v}_s\right|}{d_s} \quad (17)$$

MRF model

The MRF model aims to solve problems in which multiple moving parts are involved. The computational domain must be divided into several fluid/solid cell zones with an interfacial boundary between them. The equations of the numerical model used in this work are solved in two frames of reference, the rotating and stationary ones, as shown in Figure 2a

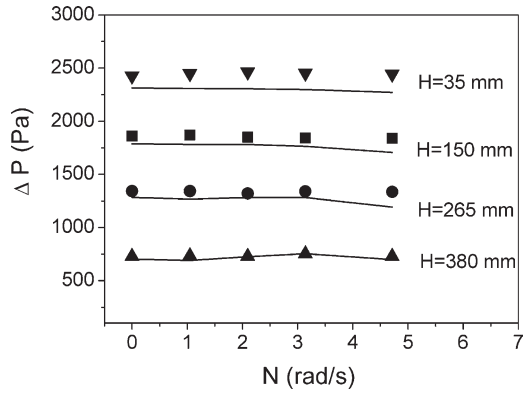

Figure 3. Comparison between predicted time-averaged bed pressure drops and experimental data at different reactor elevations (line: simulation, scatter: experimental).

where the gap between the blades and wall is magnified for the sake of clarity. Appropriate transformations between the rotating and stationary zones are preformed at the interfaces between the cell zones in order to enable flow variables in one zone to be used to calculate fluxes at the boundary of the other zone. The velocity relationship for cells between these two different reference frames is given by[38]

$$\vec{v}_{i,N}^{\,rotating} = \vec{v}_{i,N}^{\,stationary} + \varepsilon_{ijk}(\Omega_j^{stationary} - \Omega_j^{rotating})x_k \qquad (18)$$

where ε_{ijk} is the unit alternating tensor, Ω the rotational speed of the reference frame, N the agitation speed, $\vec{v}$ the velocity vector, and x_k the Cartesian coordinate component. The second term on the right side results from different rotation speeds of the frames.

The MRF approach enables unsteady-state simulations to be carried out in a pseudo-steady-state manner. It allows for considerable savings in computer resources compared to a more accurate, but time-consuming, fully time-dependent CFD simulation approach.[38]

Solution strategy

Gambit 2.2 (Ansys Inc.) was used as a grid-generation tool. The fluidized bed with a frame impeller consisted of 145,000 cells. The areas near the gas inlet, the impeller blades and the gap between the blades and wall were refined. The number of the cell elements was high enough so that an increase in it did not alter the simulation result. Figure 2b shows the grid distribution of the fluidizing system.

The numerical models were solved by *Fluent 6.2*, a commercial code of Ansys, in a 3-D unsteady framework. Turbulence was taken into account by the dispersed k–ε model, and the momentum equation for the solid phase was closed by KTGF. MRF was adopted to deal with the moving frame impeller zone in the fluidized bed. The first-order upwind method was used as the spatial discretization scheme because it yielded better convergence and required less computational effort. The implicit time integration method was used as it was usually more stable for solving a stiff equation. No-slip boundary conditions were assumed for both the gas and solid phases. The pressure outlet was set to the atmospheric one at the exit. Phase coupled SIMPLE was used to couple pressure and velocity. The time step was set to 0.0001 s because of convergence difficulties resulting from the coupling of unsteady computation and MRF in the gas–solid flow. A case took almost a month when running on an 8-core Xeon Server. To acquire enough information during the steady state fluidization, all simulations were done for 25 s of the real fluidization time.

Results and Discussion

Pressure drop and minimum fluidizing velocity

Bed pressure drop is an important parameter of a fluidized bed. Figure 3 shows the time-averaged bed pressure drop, ΔP, at different reactor elevations, H, and agitation speeds, N. The experimental data are used to validate the numerical model. To avoid temporary fluctuations in the early stage, the values of the bed pressure drops are averaged from 10 to 25 s. Unless noted otherwise, the following discussion on the simulation will be based on the statistical results corresponding to the steady fluidization period from 10 to 25 s, when the bed pressure drop fluctuates around a mean value.[39] The CFD simulations slightly underestimate the pressure drop with an average relative error of 5%, probably due to the wide particle-size distribution in the experimental work. The minimum fluidizing velocity, U_{mf}, is experimentally and numerically determined from the plots of ΔP against the fluidizing gas velocity, U_g, as shown in Figure 4. In the fluidization regime, the values of the simulated pressure drops are very close to those of the experimental ones and are independent of the agitation speed. However, in the fixed bed regime there are significant differences between them. This is consistent with the work of Taghipour et al.[40] Moreover, they decrease with increasing agitation speed. This discrepancy may be attributed to nonfluidized solids which are dominated by interparticle frictional forces and are difficult to be accurately described by the two-fluid model coupled with the Schaeffer friction model.[32] The predicted U_{mf} by CFD is about 0.37 m/s, which is somewhat lower than that of the experimental value of 0.43 m/s. Both values are independent of the agitation speed.

The effects of the agitation speed on the time-averaged bed pressure drop and minimum fluidizing velocity are negligible. This result disagrees with Leva's finding that the pressure drop decreased with increasing agitation speed for a triangular-blade agitator.[14] The reason is that the blade type dictates the capacity of the agitator to change the bed density. For axial flow impellers, particles are pressed down or lifted up by blades, which leads to an increase or a decrease

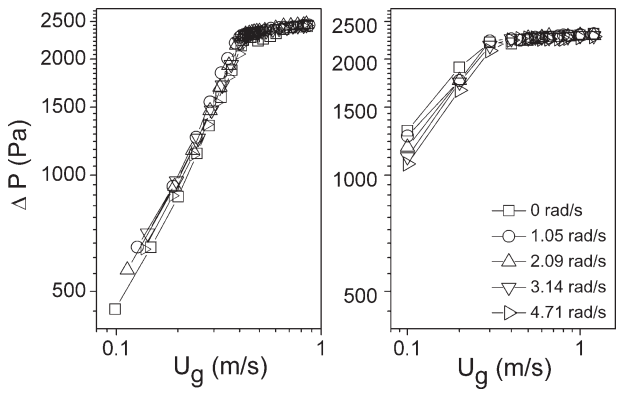

Figure 4. Effects of agitation speed and gas velocity on the experimental (left) and numerical (right) results of the time-averaged bed pressure drop at the reactor elevation of 35 mm.

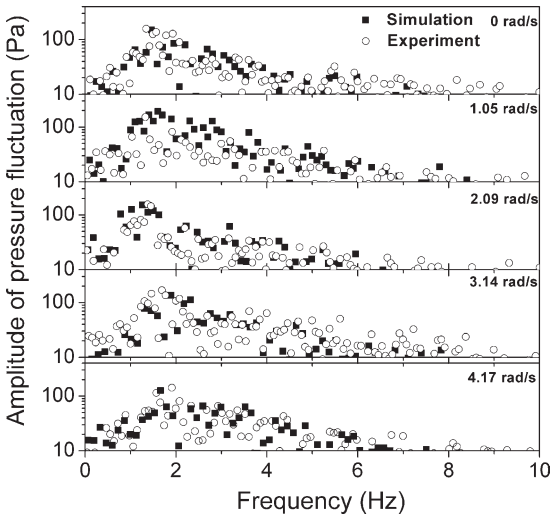

Figure 5. Comparison between simulated and experimental power spectra of pressure fluctuation at U_g = 0.85 m/s and H = 35 mm.

in the bed density. However, radial flow impellers such as the frame impeller used in this work do not have much effect on the axial components of particle velocities. Therefore, the bed pressured drop and U_{mf} may vary with the agitation speed for an axial flow impeller and remain unchanged for a radial one.

Pressure fluctuations

Pressure fluctuations are closely related to the behavior of the gas and particles in the fluidized bed. They are highly random and complicated multicomponent signals, which are composed of random or stochastic components and wave-like or sinusoidal ones.[41] Figure 5 compares the simulated and experimental power spectra of the pressure fluctuation at U_g = 0.85 m/s and H = 0.035 m. The main frequency of the simulated pressure fluctuation is close to the experimental one, with a maximum discrepancy of 0.2 Hz. This consistency further validates the numerical model. An increase in the agitation speed brings about an increase in frequency, which indicates a decrease in the bubble size.

The local pressure fluctuations are composed of several sources, including local bubble-induced fluctuations, global bed oscillations and pressure waves originating from other locations (e.g., bed surface, distributor and windbox) and propagating in the fluidized beds.[42] The bubble passage induced waves whose amplitudes are proportional to the bubble diameter are localized pressure signals, while pressure waves from other sources can be filtered out in the differential pressure signals between two nearby axial positions. As a result, it is reasonable to assume that the bubble diameter can be characterized by the amplitude of differential pressure fluctuation.[43] Figure 6 shows the time-averaged standard deviations of the differential pressure signals between two neighboring pressure probes, σ_{dP}, at a constant gas velocity of 0.85 m/s. The time-averaged bubble size can be described by σ_{dP} and is larger in the upper part of the bed. This is in accordance with the experimental work of Taghipour et al.[40] A decrease in the bubble size is also seen when the agitation speed exceeds 2.09 rad/s. The bubble size is even larger at 1.05 rad/s than that at 0 rad/s for the middle and bottom parts of the bed. Shi et al.[27] drew a similar conclusion that the fluidization quality was worse at 1.05 rad/s than that of the traditional fluidized bed. Therefore, the agitation speed should be high enough to ensure good fluidization quality.

Particle velocity distribution

The particle velocity distribution is closely associated with solids mixing. Information on the particle velocity can be provided by CFD simulation rather than by experiments because it is difficult to insert probes in the impeller area. Figure 7 shows the particle velocity distributions in the fluidized bed with different agitation speeds of the frame impeller at the superficial gas velocity of 0.85 m/s. When the agitation speed is 0 or 1.05 rad/s, the particle velocity distribution is not uniform and is similar to that of free fluidization. As the agitation speed increases, it becomes more uniform and the particle velocities around bubbles are also reduced.

Solid mixing is controlled by two main mechanisms: gross circulation and internal circulation.[44] The influence of the agitation speed on the gross circulation at the bed scale can be ignored, because the frame impeller is a radial flow one. The latter does not contribute much to the axial velocity of particles. However, internal circulations are induced by bubble passage at a bubble scale and are influenced by the shear force generated by the rotation of the impeller blades. The fluidization performance is improved for an agitation speed higher than 2.09 rad/s, due to reduced internal circulations.

Solid volume fraction distribution

Poor gas–solid fluidization quality can be caused by agglomeration or accumulation of particles which may lead to hot spots in an industrial reactor. A uniform distribution of solids with small or even no bubbles is preferred. Incorporation of a frame impeller in a traditional fluidized bed is supposed to reduce the bubble diameter. The distribution of the solid volume fraction calculated by CFD method is discussed in this section.

The fluidized bed used in this work can be divided into several imaginary zones according to the bed elevations of four measuring points. Figure 8 shows the predicted fluctuation of the volume-averaged solid volume fraction vs. the agitation speed of the frame impeller at a superficial gas velocity of 0.85 m/s in the following zones: 35–150, 150–265, and 265–380 mm of the bed elevation, respectively.

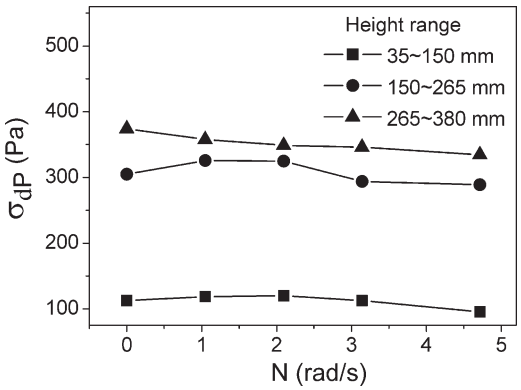

Figure 6. Experimental standard deviations of differential pressure fluctuations between neighboring probes at a superficial gas veocity of 0.85 m/s.

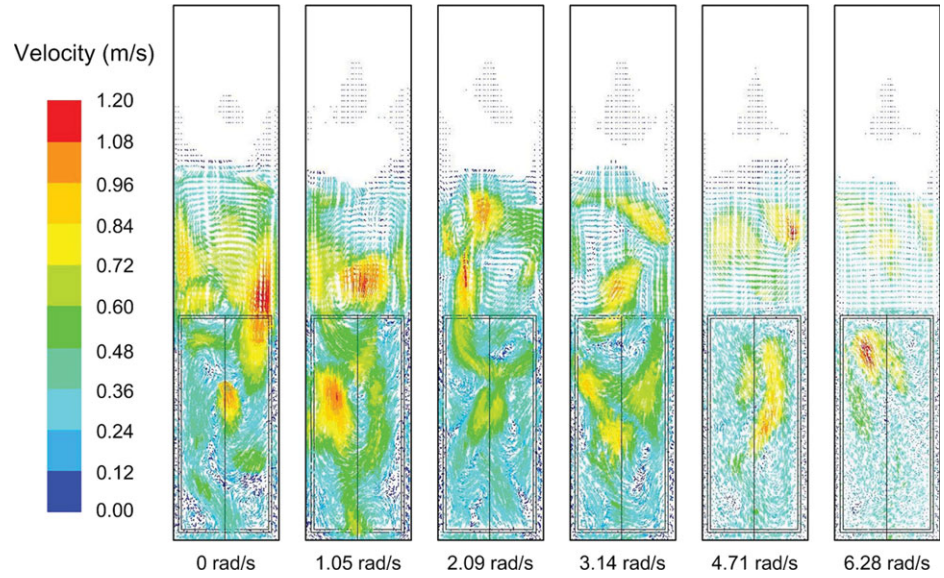

Figure 7. Particle velocity vector profiles for different agitation speeds at a fluidization time of 25 s (U_g = 0.85 m/s).

[Color figure can be viewed in the online issue, which is available at wileyonlinelibrary.com.]

Fluctuations become smoother at the lower reactor elevation and the fluidization quality better. The fluctuations in the upper part of the bed are more intense due to the dynamics of coalescence and eruption of bubbles around the bed surface.[45] The positive effect of the agitation on the solid volume fraction fluctuation becomes more pronounced when its speed exceeds 2.09 rad/s.

Figure 9 shows the instantaneous solid volume fraction contour in the vertical mid-plane at the beginning of fluidization (U_g = 0.85 m/s) for an agitation speed of 0 and 4.71 rad/s, respectively. The bed rapidly expands during the fluidization time smaller than 1.2 s. Thereafter, big bubbles break up at the surface of the bed and particles entrained by bubbles come back to gross circulation near the wall. In the initial period of fluidization particles have to overcome interparticle locking, which may result in slug fluidization. After the break-up of big bubbles at the surface, agitation significantly improves the uniformity of the solid volume fraction distribution.

Figure 10 shows the solid volume fraction distribution for steady fluidization in the vertical mid-plane (U_g = 0.85 m/s). Bubbles break up and coalesce continuously as the fluidization proceeds. The bubble coalescence process can be observed at low agitation speeds, that is, 1.05 rad/s. Small bubbles formed at the bottom of the bed rise upwards and deform due to particle–particle interactions. Neighboring bubbles coalesce because lower bubbles are attracted by low pressure in the wake of the upper ones.[46]

As the agitation speed exceeds 2.09 rad/s, the bubble diameter decreases and the effect of the frame impeller on the fluidization quality is more obvious. According to Shi et al.,[27] fluidization was worsened at 1.05 rad/s, which is consistent with our work. The agitation speed of the frame impeller should be high enough, say, higher than 2.09 rad/s, to uniformly distribute solids. The sizes of bubbles can be reduced by the intensive shear stress provided by agitation.[4,5]

The uniformity of the solid volume fraction distribution at the superficial gas velocity of 0.85 m/s can be quantified by its time-averaged standard deviation, $\sigma_{\varepsilon s}$, as shown in Figure 11. The $\sigma_{\varepsilon s}$ is low at the bottom of the bed and increases with the reactor elevation, as a result of the bubble size increase in the fluidized bed.[47] Beneath the reactor elevation of 150 mm, it increases with increasing agitation

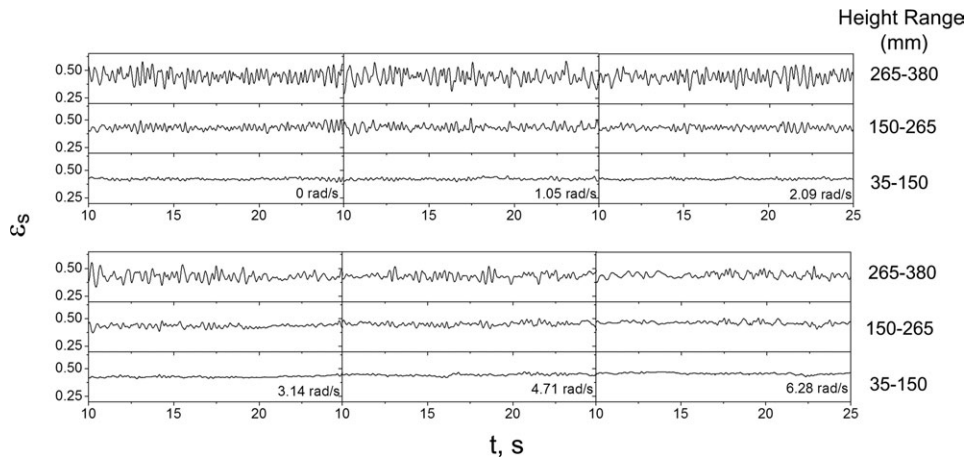

Figure 8. Simulated volume-averaged fluctuations of solid volume fraction at different reactor elevations vs. agitation speed (U_g = 0.85 m/s).

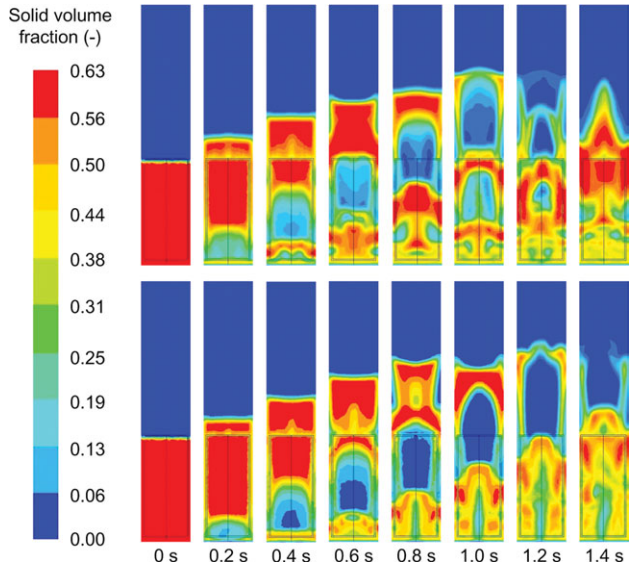

Figure 9. Instantaneous solid volume fraction contour in the vertical mid-plane vs. fluidization time (top: N = 0 rad/s; bottom: N = 4.71 rad/s; U_g = 0.85 m/s).

[Color figure can be viewed in the online issue, which is available at wileyonlinelibrary.com.]

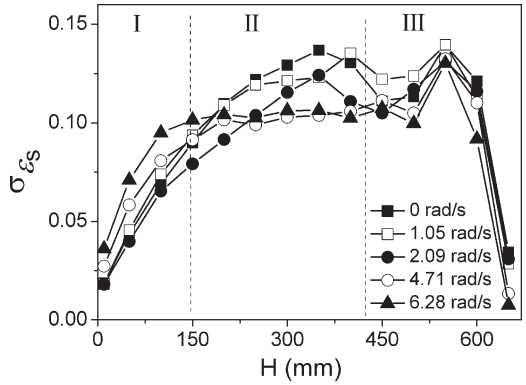

Figure 11. Simulated time-averaged standard deviations of solid volume fraction for different agitation speeds (U_g = 0.85 m/s).

speed (>2.09 rad/s). As the reactor elevation is higher; however, the opposite correlation is observed between the standard deviation and the agitation speed. When the reactor elevation exceeds the upper edge of the impeller (>400 mm), $\sigma_{\varepsilon s}$ is almost no longer affected by the agitation speed.

According to the agitation effect of the frame impeller on the fluidization performance (Figures 10 and 11), the whole bed can be divided into three zones: inlet zone (I), agitated fluidization zone (II), and free fluidization zone (III). In the inlet zone (H < 150 mm), the solid distribution is uniform with small bubbles[24] due to the gas distributor, as shown in Figure 10. In this zone, the impeller has little or a negative influence (higher $\sigma_{\varepsilon s}$) on the fluidization performance when the agitation speed exceeds 2.09 rad/s (Figure 11). The reactor elevation ranging from 150 mm to the top edge of the impeller (400 mm) is called agitated fluidization zone in which a large part of the frame impeller is located. The fluidization performance is significantly improved at higher agitation speed (N > 2.09 rad/s). This is because an intensive shear stress decreases bubble sizes. The free fluidization zone is between the top edge of the impeller and the bed surface. The impeller does not reach this zone. As a result, the effect of the agitation speed becomes negligible.

At high agitation speed, the uniformity of the solid distribution is improved in the agitated fluidization zone whereas it is worsened in the inlet zone. This can be explained by the radial solid volume fraction distribution shown in Figure 12 (U_g = 0.85 m/s). At the reactor elevation of 50 mm (inlet zone), the uniformity of the solid volume

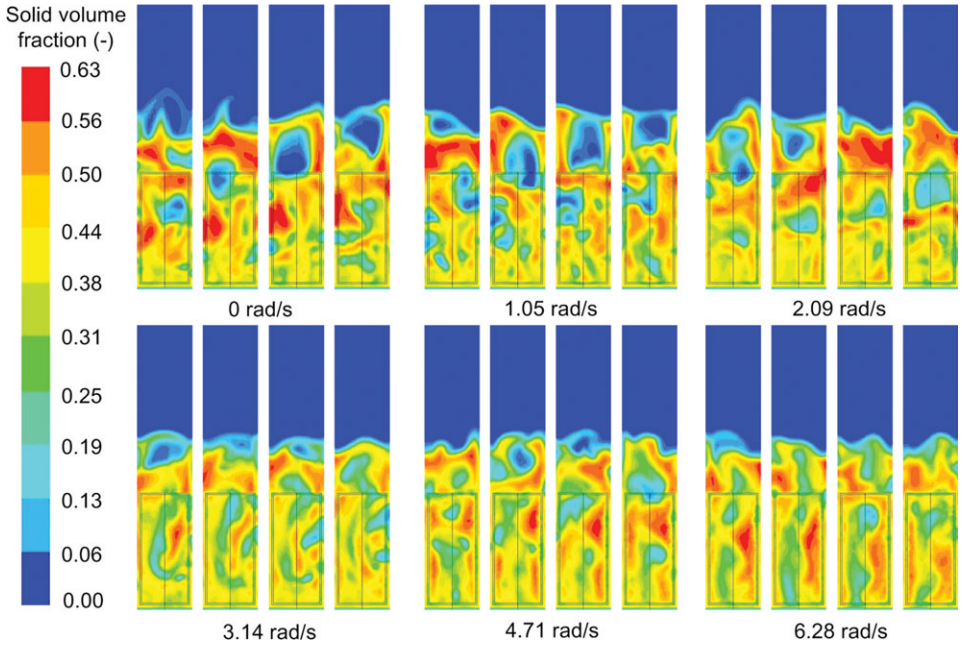

Figure 10. Solid volume fraction distribution of steady fluidization at the fluidization time of 24.4, 24.5, 24.6, and 24.7 s in the vertical mid-plane for different agitation speeds (U_g = 0.85 m/s).

[Color figure can be viewed in the online issue, which is available at wileyonlinelibrary.com.]

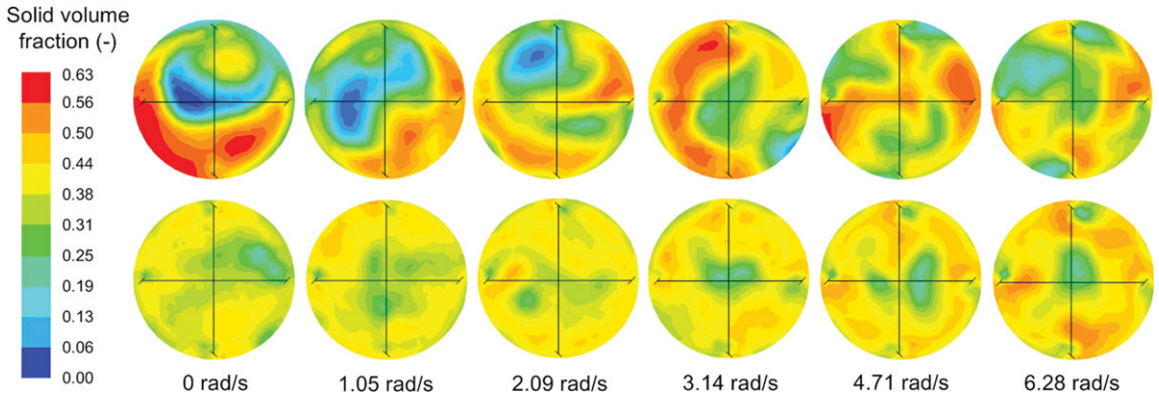

Figure 12. Solid volume fraction distribution in horizontal planes at a fluidization time of 20 s for different agitation speeds. (top: H = 350 mm; bottom: H = 50 mm; U_g = 0.85 m/s).

[Color figure can be viewed in the online issue, which is available at wileyonlinelibrary.com.]

fraction distribution is worsened with increasing agitation speed, especially when the latter is 6.28 rad/s. The rotating direction is anticlockwise and there is a high solid volume fraction at the leading edge of the blades. A similar phenomenon of particle accumulation caused by the shear force also appears in bladed solid mixers.[48,49] The agitation speed of the frame impeller is limited to 6.28 rad/s due to its big and negative impact on the fluidization performance. On the contrary, the fluidization is improved for a higher agitation speed at the reactor elevation of 350 mm (agitated fluidization zone), where big bubbles are formed due to bubble coalescence and the fluidization performance is not as good as that in the inlet zone. The rotation of the impeller can reduce bubble size, resulting in a more homogeneous solid volume fraction distribution. Meanwhile, particle accumulation at the leading edge of the blades is found to be negligible.

Conclusions

A 3-D time-dependent CFD model based on the Eulerian–Eulerian two-fluid model incorporating the KTGF is developed to describe a gas–solid fluidized bed with a frame impeller for olefin polymerization. The MRF method is used to deal with the agitation of the impeller. The numerical model is validated experimentally in terms of the bed pressure drop and pressure fluctuation.

The effect of the agitation speed on the minimum fluidizing velocity and bed pressure drop can be ignored, because the frame impeller is a radial flow one and has little contribution to the lift force for particles. An increase in the agitation speed brings about a decrease in bubble size.

Fluidization performance is improved by the incorporation of the frame impeller. Internal circulations are induced by the bubble passage at the scale of bubble diameter and are reduced by the rotation of the impeller blades. The influence is more significant when the agitation speed is large enough, say, higher than 2.09 rad/s.

The whole fluidized bed can be divided into three zones: inlet zone, agitated fluidization zone, and free fluidization zone. The effect of the gas distributor is dominant in the inlet zone, while the fluidization performance can be enhanced by the rotation of the frame impeller in the agitated fluidization zone. For the free fluidization zone where no impeller blades exist, the influence of the agitation speed on the fluidization quality is not significant.

Acknowledgments

This work was supported financially by the National High Technology Research and Development Program of China (2012AA040305), Program for Changjiang Scholars and Innovative Research Team in University (IRT0942), and the Fundamental Research Funds for the Central Universities.

Notation

C_D = drag coefficient, dimensionless
d_s = particle diameter, m
e_{ss} = particle–particle restitution coefficient, dimensionless
g = gravitational acceleration, m/s^2
$g_{0,ss}$ = radial distribution function for particle collisions
H = reactor elevation, mm
$\bar{\bar{I}}$ = identity matrix
I_{2D} = second invariant of the deviatoric stress tensor
K_{gs} = interphase exchange coefficient, kg/(m^2·s)
$K_{\Theta s}$ = diffusion coefficient for granular energy, kg/(m·s)
N = agitation speed, rad/s
P = pressure, Pa
P_s = solids pressure, Pa
Re_s = solid phase Reynolds number, dimensionless
t = physical fluidization time, s
U_g = superficial gas velocity, m/s
$\vec{v}$ = velocity vector, m/s
x_k = Cartesian coordinate component

Greek letters

ε = volume fraction, dimensionless
ε_{ijk} = unit alternating tensor
ϕ = transfer rate of kinetic energy, kg/(s^3·m)
$\gamma\Theta_s$ = collisional dissipation of energy, kg/(m·s^3)$^{-1}$
φ = angle of internal friction, °
λ_s = solids bulk viscosity, kg/(m·s)$^{-1}$
μ_s = solids shear viscosity, kg/(m·s)$^{-1}$
$\vec{v}$ = velocity vector, m/s
Θ_s = granular temperature, m^2/s^2
ρ = density, kg/m^3
$\bar{\bar{\tau}}$ = shear stress, N/m^2
σ = standard deviation
Ω = rotational speed of the reference frame, rad/s

Subscripts

dp = differential pressure fluctuation
εs = solid volume fraction
g = gas phase
i = general index
mf = minimum fluidization
N = agitation speed
s = granular (solid) phase
P = Pressure

Literature Cited

1. Godard K, Richardson JF. The use of slow speed stirring to initiate particulate fluidisation. *Chem Eng Sci*. 1969;24:194–195.
2. Reina J, Velo E, Puigjaner L. Fluidization of waste-wood particles with mechanical agitation of the bed. *Ind Eng Chem Res*. 2001;40:393–397.
3. Kim J, Han GY. Effect of agitation on fluidization characteristics of fine particles in a fluidized bed. *Powder Technol*. 2006;166:113–122.
4. Watano S, Sato Y, Miyanami K, Murakami T, Nagami N, Ito Y, Kamata T, Oda N. Scale-up of agitation fluidized bed granulation. II. Effects of scale, air flow velocity and agitator rotational speed on granule size, size distribution, density and shape. *Chem Pharm Bull*. 1995;43:1217–1220.
5. Watano S, Sato Y, Miyanami K, Ito Y, Kamata T, Oda N. Scale-up of agitation fluidized bed granulation. III. Effects of powder feed weight and blade angle on granule size, density and shape. *Chem Pharm Bull*. 1995;43:1224–1226.
6. Daud WRW. Fluidized bed dryers-recent advances. *Adv Powder Technol*. 2008;19:403–418.
7. Martins PM, Rocha F. The role of diffusional resistance on crystal growth: interpretation of dissolution and growth rate data. *Chem Eng Sci*. 2006;61:5686–5695.
8. Beeckmans JM, Yu Z. Continuous separation of solids in a mechanically fluidized bed. *Powder Technol*. 1992;70:77–81.
9. Li F, Feng LF, Gu XP, Wang K, Liu B. Pressure drop in gas-solid stirred fluidized bed. *J Chem Eng Chin Univ*. 2002;16:384–388.
10. Feng LF, Zhang WF, Wang JJ, Gu XP, Wang K. Pressure fluctuation in the gas-solid agitated fluidized bed. *J Zhejiang Univ (Eng Sci)*. 2007;41:524–528.
11. Wang JJ, Zhang WF, Feng LF, Gu XP. Wavelets analysis of pressure fluctuation in agitated fluidized bed. *J Chem Ind Eng (China)*. 2006;57:2854–2859.
12. Ma QS, Feng LF, Chen PF, Wang K. Studies on the power consumption for agitated fluidized bed. *Chem Eng (China)*. 2001;29:20–25.
13. Reed TM, Fenske MR. Effects of agitation on gas fluidization of solids. *Ind Eng Chem*. 1955;47:275–282.
14. Leva M. Pressure drop and power requirements in a stirred fluidized bed. *AIChE J*. 1960;6:688–692.
15. Murthy JSN, Sekhar PC, Haritha K, Balaram P, Anjani S. Hydrodynamic characteristics of stirred gas-solid fluidized beds. *J Inst Eng (India)*. 2003;83:39–44.
16. Murthy JSN, Sekhar PC. Studies on hydrodynamics of mechanically stirred fluidised beds-a statistical approach. *Ind Chem Eng Sect A*. 2004;46:84–89.
17. Makishima S, Shirai T. Experimental study on the power requirements for agitating beds of solid particles, and proposal of a new model. *J Chem Eng Jpn*. 1968;1:168–174.
18. Makishima S, Shirai T. Experimental study of the power numbers for agitating beds of solid particles with multiple blades and upward streams of gas less than U_{mf}. *J Chem Eng Jpn*. 1968;1:175–180.
19. Makishima S, Shirai T. Power requirements for agitating air-fluidised beds. *J Chem Eng Jpn*. 1969;2:224–228.
20. Zimmermann S, Taghipour F. CFD modeling of the hydrodynamics and reaction kinetics of FCC fluidized-bed reactors. *Ind Eng Chem Res*. 2005;44:9818–9827.
21. Chalermsinsuwan B, Piumsomboon P, Gidaspow D. Kinetic theory based computation of PSRI riser: Part I-Estimate of mass transfer coefficient. *Chem Eng Sci*. 2009;64:1195–1211.
22. van Wachem B, Sasic S. Derivation, simulation and validation of a cohesive particle flow CFD model. *AIChE J*. 2008;54:9–19.
23. Xu BH, Yu AB. Numerical simulation of the gas-solid flow in a fluidized bed by combining discrete particle method with computational fluid dynamics. *Chem Eng Sci*. 1997;52:2785–2809.
24. Lu HL, He YR, Gidaspow D. Hydrodynamic modelling of binary mixture in a gas bubbling fluidized bed using the kinetic theory of granular flow. *Chem Eng Sci*. 2003;58:1197–1205.
25. Kim J, Han GY. Simulation of bubbling fluidized bed of fine particles using CFD. *Korean J Chem Eng*. 2007;24:445–450.
26. *FLUENT 6.2 user's guide*. Lebanon, NH: Fluent Inc., 2005.
27. Shi DP, Luo ZH, Guo AY. Numerical simulation of the gas-solid flow in fluidized-bed polymerization reactors. *Ind Eng Chem Res*. 2010;49:4070–4079.
28. Ding JM, Gidaspow D. A bubbling fluidization model using kinetic theory of granular flow. *AIChE J*. 1990;36:523–538.
29. Gidaspow D, Bezburuah R, Ding J. Hydrodynamics of circulating fluidized beds: Kinetic theory approach. In: *Fluidization VII*. Proceedings of the 7th Engineering Foundation Conference on Fluidization, Brisbane, Australia, 1992:75–82.
30. Lun CKK, Savage SB, Jeffrey DJ, Chepurniy N. Kinetic theories for granular flow: inelastic particles in couette flow and slightly inelastic particles in a general flowfield. *J Fluid Mech*. 1984;140:223–256.
31. Ogawa S, Umemura A, Oshima N. On the equations of fully fluidized granular materials. *ZAMP*. 1980;31:483–493.
32. Schaeffer DG. Instability in the evolution equations describing incompressible granular flow. *J Diff Eq*. 1987;66:19–50.
33. Wen CY, Yu YH. Mechanics of fluidization. *Chem Eng Prog Symp Ser*. 1966;62:100–111.
34. Gidaspow D. *Multiphase flow and fluidization: Continuum and kinetic theory description*. New York: Academic Press; 1994.
35. Syamlal M, O'Brien T. Computer simulation of bubbles in a fluidized bed. *AIChE Symp Ser*. 1989;85:22–31.
36. Asegehegn TW, Schreiber M, Krautz HJ. Numerical simulation and experimental validation of bubble behavior in 2D gas-solid fluidized beds with immersed horizontal tubes. *Chem Eng Sci*. 2011;66:5410–5427.
37. Sanyal J, Cesmebasi E. On the effect of various momentum transfer coefficient models on bubble dynamics in a rectangular gas fluidized bed. *Chem Eng Sci*. 1994;49:3955–3966.
38. Akiti O, Armenante PM. Experimentally-validated micromixing-based CFD model for fed-batch stirred-tank reactors. *AIChE J*. 2004;50:566–577.
39. Ergun S. Fluid flow through packed columns. *Chem Eng Prog*. 1952;48:89–94.
40. Taghipour F, Ellis N, Wong C. Experimental and computational study of gas-solid fluidized bed hydrodynamics. *Chem Eng Sci*. 2005;60:6857–6867.
41. Saxena SC, Waghmare B. Investigations of pressure fluctuation history records of gas-solid fluidized beds. *Int J Energy Res*. 2000;24:495–502.
42. Bi HT. A critical review of the complex pressure fluctuation phenomenon in gas-solids fluidized beds. *Chem Eng Sci*. 2007;62:3473–3493.
43. Zhang YM, Grace JR, Bi XT, Lu CX, Shi MX. Effect of louver baffles on hydrodynamics and gas mixing in a fluidized bed of FCC particles. *Chem Eng Sci*. 2009;64:3270–3281.
44. Norouzi HR, Mostoufi N, Mansourpour Z, Sotudeh-Gharebagh R, Chaouki J. Characterization of solids mixing patterns in bubbling fluidized beds. *Chem Eng Res Des*. 2011;89:817–826.
45. Busciglio A, Vella G, Micale G, Rizzuti L. Analysis of the bubbling behaviour of 2D gas solid fluidized beds: Part II. Comparison between experiments and numerical simulations via digital image analysis technique. *Chem Eng J*. 2009;148:145–163.
46. Hosseini SH, Ahmadi G, Rahimi R, Zivdar M, Esfahany MN. CFD studies of solids hold-up distribution and circulation patterns in gas-solid fluidized beds. *Powder Technol*. 2010;200:202–215.
47. Owoyemi O, Lettieri P. Experimental validation of eulerian-eulerian simulations of rutile industrial powders. *Ind Eng Chem Res*. 2005;44:9996–10004.
48. Remy B, Khinast JG, Glasser BJ. Discrete element simulation of free flowing grains in a four-bladed mixer. *AIChE J*. 2009;55:2035–2048.
49. Remy B, Canty TM, Khinast JG, Glasser BJ. Experiments and simulations of cohesionless particles with varying roughness in a bladed mixer. *Chem Eng Sci*. 2010;65:4557–4571.

Manuscript received July 30, 2011, and revision received July 12, 2012.